ChemPhysChem

Research Article
doi.org/10.1002/cphc.202200561

Chemistry Europe
European Chemical Societies Publishing

www.chemphyschem.org

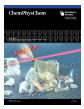

Conformer-selective Photodynamics of $TrpH^+$–H_2O

Franco Molina,[a, f] Jordan Dezalay,[a] Jun-ichi Tabata,[b, e] Satchin Soorkia,[a] Michel Broquier,[a] Keisuke Hirata,*[b, c, d] Shun-Ichi Ishiuchi,*[b, c, d] Masaaki Fujii,*[b, d, e] and Gilles Grégoire*[a, d]

The photodynamics of protonated tryptophan and its mono hydrated complex $TrpH^+$–H_2O has been revisited. A combination of steady-state IR and UV cryogenic ion spectroscopies with picosecond pump-probe photodissociation experiments sheds new lights on the deactivation processes of $TrpH^+$ and conformer-selected $TrpH^+$–H_2O complex, supported by quantum chemistry calculations at the DFT and coupled-cluster levels for the ground and excited states, respectively. $TrpH^+$ excited at the band origin exhibits a transient of less than 100 ps, assigned to the lifetime of the excited state proton transfer (ESPT) structure. The two experimentally observed conformers of $TrpH^+$–H_2O have been assigned. A striking result arises from the conformer-selective photodynamics of $TrpH^+$–H_2O, in which a single water molecule inserted in between the ammonium and the indole ring hinders the barrierless ESPT reaction responsible for the ultra-fast deactivation process observed in the other conformer and in bare $TrpH^+$.

Introduction

Tryptophan (Trp) is the dominant natural fluorophore in proteins, giving its high UV absorbance and broad emission spectrum.[1] The emission of tryptophan is very sensitive to its vicinal environment and is often used as a local probe of protein conformational changes.[2] Trp fluorescence can be quenched by remote charged groups like negatively charged disulfide group or protonated ammonium and residues[3] and also by the exposure to water in solution.[4] Interestingly, the bare amino acids already exhibits a rich photochemistry, evidenced by the large variation of lifetime and quantum yield as a function of the solvent, pH and its conformation.[5,6] A deep understanding of the photophysics of molecular systems indeed requires an optimal degree of control of the initial and final states of the reaction, which can be achieved in the gas phase through the combination of mass spectrometry with laser spectroscopy of conformer-selected molecular systems. Cold ion spectroscopy has emerged for structural determinations and excited state properties of biomolecules. Cryogenic cooling ensures the suppression of inhomogeneous broadening and allows recording conformer-selected spectroscopy that can be directly compared to quantum chemistry calculations. Cold ion photodissociation has now been developed as a new tool for structural determination and photophysics studies of biomolecules through IR and UV spectroscopy, respectively and we shall refer the interested reader to recent reviews.[7,8]

Protonated tryptophan ($TrpH^+$) symbolizes a benchmark molecular system for UV photodissociation spectroscopy. The manifold of low-lying excited states with charge transfer character in the vicinity of the locally excited $\pi\pi^*$ state prompts a complex photochemistry, evidenced by ultrashort excited state lifetime,[9] UV specific photofragmentation channels including H-loss and C_α–C_β bond cleavage[10] with several deactivation processes in competition. The broad excitation spectrum at the band origin of $TrpH^+$ reported by Boyarkin *et al.*[11] has been theoretically assigned to a barrierless excited state proton transfer (ESPT) from the ammonium group to the indole side chain.[12] ESPT has been often evoked to rationalize the photophysics of protonated aromatic amino acids and derivatives, short peptides and neurotransmitters. It implicates a proton transfer from the ammonium group toward the aromatic ring, leading to an excited state structure which lies at lower energy than the adiabatic excitation energy of the $\pi\pi^*$ state. In the ESPT form, the C_α–C_β bond elongates due to a larger contribution of its antibonding orbital, eventually leading to the cleavage of the bond, as observed for protonated tyrosine and phenylalanine,[13] noradrenaline[14] and

[a] F. Molina, Dr. J. Dezalay, Dr. S. Soorkia, Dr. M. Broquier, Dr. G. Grégoire
Université Paris-Saclay, CNRS, Institut des Sciences Moléculaires d'Orsay, 91405 Orsay, France
E-mail: gilles.gregoire@universite-paris-saclay.fr
[b] J.-i. Tabata, Dr. K. Hirata, Prof. S.-I. Ishiuchi, Prof. M. Fujii
Laboratory for Chemistry and Life Science, Institute of Innovative Research, Tokyo Institute of Technology,
4259 Nagatsu-ta-cho, Midori-ku, Yokohama, 226-8503, Japan
E-mail: hirata.k.ai@m.titech.ac.jp
ishiuchi.s.aa@m.titech.ac.jp
mfujii@res.titech.ac.jp
[c] Dr. K. Hirata, Prof. S.-I. Ishiuchi
Department of Chemistry, School of Science, Tokyo Institute of Technology, 2-12-1 4259 Ookayama, Meguro-ku, Tokyo, 152-8550, Japan
[d] Dr. K. Hirata, Prof. S.-I. Ishiuchi, Prof. M. Fujii, Dr. G. Grégoire
Tokyo Tech World Research Hub Initiative (WRHI), Institute of Innovation Research, Tokyo Institute of Technology
4259, Nagatsuta-cho, Midori-ku, Yokohama, 226-8503, Japan
[e] J.-i. Tabata, Prof. M. Fujii
School of Life Science and Technology, Tokyo Institute of Technology,
4259 Nagatsu-ta-cho, Midori-ku, Yokohama, 226-8503, Japan
[f] F. Molina
INFIQC (CONICET-UNC). Departamento de Fisicoquímica, Fac. de Ciencias Químicas. Centro Láser de Ciencias Moleculares.
Universidad Nacional de Córdoba, Ciudad Universitaria
Pabellón Argentina, X5000HUA Córdoba, Argentina

Supporting information for this article is available on the WWW under https://doi.org/10.1002/cphc.202200561

adrenaline.[15] The UV-specific dissociation of the C_α–C_β bond is generally in competition with other fragmentation channels as those commonly observed in CID or IRMPD experiments.[16] Internal conversion to the ground state can indeed occur along the ESPT path leading to the detection of the NH_3 loss channel like for protonated tryptophan,[11] tyramine[17] and dopamine.[18]

The excited state dynamics of $TrpH^+$ has been studied at 266 nm, *i.e.* with 0,3 eV of excess energy in the $\pi\pi^*$ state. Femtosecond pump-probe photodissociation dynamics has revealed two time constants of 400 fs and 15 ps,[19] measured at room temperature. In this spectral region, the H-loss photodissociation channel is opened (onset at 275 nm),[20] which is triggered by the coupling with the $\pi\sigma^*$ state repulsive along the N–H stretch of the ammonium group following electron transfer from the indole moiety.[21] However, the bi exponential decay observed for $TrpH^+$ could not be firmly assigned, being due to the contribution of several conformers present at room temperature and/or to the lifetime of different excited states ($\pi\pi^*$, $\pi\sigma^*$) which are coupled at the excitation energy (266 nm) used in the pump-probe photodissociation experiment. The lack of conformer selectivity and the large excess energy brought by the 266 nm pump laser precluded a conclusive assignment. In order to get a precise control of the experimental conditions, we have recently shown that tunable picosecond laser provides a good compromise between spectral (10 cm^{-1} bandwidth) and temporal (16 ps cross-correlation) resolutions that enables recording mode-specific and conformer-selected excited state lifetimes of cold biomolecules.[22]

While $TrpH^+$ displays unresolved excitation spectrum at the band origin, Mercier *et al.*[23] reported that the addition of two water molecules lengthens the excited state lifetime, underlined by a well-resolved vibronic spectrum of $TrpH^+$–$(H_2O)_2$. Such drastic hydration effect has recently been observed in protonated dopamine solvated by three water molecules.[18] In both cases, calculations predict ESPT from the ammonium to the aromatic ring with no or low energy barrier, providing an efficient and fast deactivation pathway. In water clusters, due to the strong electrostatic interaction, the protonated ammonium group gets solvated by the first solvent molecules, impeding the direct interaction of the charged group with the ring and thus blocking the ESPT reaction.[24]

We here report new experimental results on the photophysics of $TrpH^+$ and $TrpH^+$–H_2O complex, supported by quantum chemistry calculations. We have investigated the photodynamics of $TrpH^+$ at the band origin and measured the excited state lifetime of the ESPT form. The photophysics of $TrpH^+$–H_2O has been revisited. UV photodissociation (UVPD), IR-UV hole burning and pump-probe photodissociation spectroscopies are reported showing that two conformers with photophysical properties drastically different contribute to the experimental spectra. In particular, the lengthening of the excited state lifetime that has been previously observed in $TrpH^+$–$(H_2O)_2$ is already effective in a conformer-selected mono hydrated complex. Besides, this $TrpH^+$–H_2O conformer with a nanosecond excited state lifetime has a specific UV photofragmentation channel, m/z 131, issued from the C_α–C_β bond cleavage. This specific fragmentation channel closes 300 cm^{-1} above the band origin and is replaced by the water and ammonia loss (m/z 188) as observed for the other conformer.

Results and Discussion

Excited-State Lifetime of the ESPT form of $TrpH^+$

At the band origin (284 nm), the main UV photofragment corresponds to the ammonia loss channel at m/z 188. Other minor primary photofragments are detected at m/z 130, m/z 132 and m/z 159 (see Fig SI1a). All these photofragments are promptly formed following UV excitation (within the 100 ns time limit of the extraction of the ions from the QIT). When the extraction time of the ions following the UV excitation is increased to the millisecond range, the intensity of all photofragments is constant except for m/z 188 which has disappeared. Instead, a new fragment at m/z 146 is observed, which indeed corresponds to the loss of CH_2CO after the ammonia loss (Figure S1b).[25] The dissociation chemistry of $TrpH^+$ in the ground state has already been investigated theoretically and spectroscopically. Intramolecular proton transfer from the ammonium to the indole ring has the lowest energy barrier, in the order of 12–15 kcal/mol, about 10 kcal/mol lower than the energy of the transition state leading to the loss of ammonia. The reaction coordinate for the loss of ammonia from $TrpH^+$ in the ground state involves nucleophilic attack from the C_γ position of the indole chain,[26] resulting in a spirocyclopropane structure which has been clearly assigned through IRMPD spectroscopy.[27] Subsequently, CH_2CO is lost to yield the m/z 146 fragment. It can be concluded that when excited at the band origin, $TrpH^+$ dissociates after internal conversion to the ground state as observed in low-energy CID or IRMPD experiments.

Here, we report the excited state dynamics of $TrpH^+$ excited at the band origin which precedes the return to the ground state. In order to record the pump-probe photodissociation spectroscopy, the extraction time of the ions from the QIT is set at 20 ms, so the main UV photofragment is m/z 146. Two probe wavelengths have been used to monitor the excited state dynamics. When the probe is set at 650 nm, the m/z 146 fragmentation channel is depleted (negative ion peak) and a concomitant apparition of ion signal at m/z 188 (positive ion peak, see Figure 1a) is observed. The negative peak indicates depletion of the fragmentation channel normally observed with the pump laser only, while the positive peak show the fragment generated by the pump + probe scheme. The time evolution of the m/z 146 and m/z 188 fragments as a function of the pump-probe delay is reported in Figure 1b. For both fragments, the transient is fitted by an exponential decay function with a short time constant of 40 ps ± 2 ps. The extraction time of the ions from the QIT being at 20 ms, none m/z 188 fragment could be detected if issued from a statistical dissociation process in the ground electronic state. The apparition of the m/z 188 fragment can only be due to a direct dissociation from an excited state that triggers the prompt C_α-N cleavage, and not to a

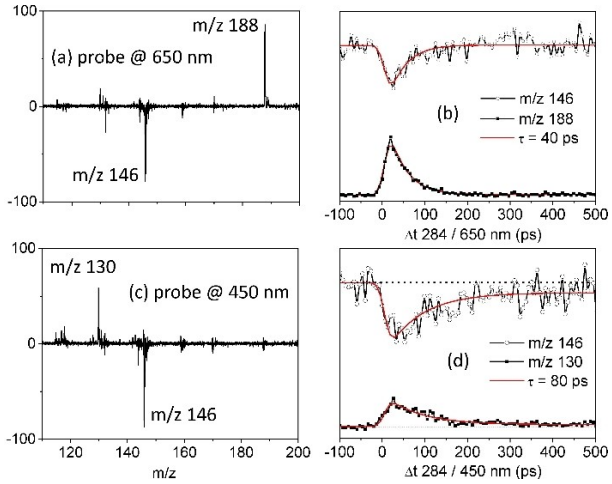

Figure 1. (a, c) difference mass spectrum [(pump + probe) – pump only] of $TrpH^+$ as a function of the probe wavelength. (b, d) time evolution of the photofragment signals as a function of the pump/probe delay for two probe wavelengths.

dissociation in the ground electronic state following internal conversion.[28] It is noteworthy that m/z 188 produced through the pump-probe scheme was already detected in the fs pump-probe dynamics of room-temperature $TrpH^+$ excited at 266 nm with a probe set at 800 nm.[19] For sake of comparison, we have recorded the transient at 266 nm which exhibits a time constant of 22 ps ± 2 ps. The smaller time constant of 15 ps is in agreement with the 22 ps found here for cold $TrpH^+$ due to the increase of internal energy of $TrpH^+$ at 300 K.[22]

When the probe wavelength is set to 450 nm, the 2-color photodissociation mass spectrum changes completely with the apparition of the m/z 130 fragment instead of the m/z 188 (Figure 1c). Figure SI2 reports the branching ratio of these two fragmentation channels as a function of the probe wavelength from 650 nm to 450 nm recorded at zero pump-probe delay. There is a clear breakdown of the intensity of the m/z 188 channel at about 525 nm with the formation of the m/z 130 at shorter wavelengths. Interestingly, the time constants recorded for the two excitation wavelengths (284 nm and 266 nm) with the probe laser set at 450 nm are systematically longer than those recorded using a probe at 650 nm (Figure SI3). Besides, a constant 2-color signal of low intensity is seen (on the 500 ps time scale), which was not detected with the 650 nm probe laser. These two results points out the influence of the probe wavelength upon the 2-color photodissociation signal of $TrpH^+$ which is certainly related to the excitation of different states by the probe photon.[39,40,41]

The broadening of the excitation spectrum of $TrpH^+$ implies an ultra-short lifetime of the locally excited ππ* state that should take hold in the femtosecond time range, so the time constant measured here about a few tens of ps must be assigned to the lifetime of another excited state. Besides, the evolution of the transient signal with the probe wavelength suggests that the observed dynamics is influenced by a resonant condition of the probe photon from this excited state. Excited state calculations have thus been performed to rationalize these transients.

As already reported by Pereverzev *et al.*,[32] $TrpH^+$ adopt two main conformations at cryogenic temperature, conformers A and B, which differ from the orientation of the amino acid moiety above the indole ring. In any case, the ammonium interacts above the indole ring while the carboxylic acid group is standing either backward (conformer A) or above the five-membered indole ring (conformer B) of the UV chromophore. Optimization of the ππ* state of these $TrpH^+$ conformers leads to a barrierless excited state proton transfer.[12] Interestingly, the ESPT form is a minimum of the potential energy surface (PES), with an adiabatic excitation energy calculated at 3.58 eV, so about 0,8 eV below the band origin. In this ESPT form, the protonated indole ring keeps a planar geometry and the energy gap with the ground electronic state is larger than 2 eV, preventing a direct path to internal conversion to the ground state. The two time constants extracted from the fit of the transient signals recorded at 284 nm with two probe wavelengths impede the excited state lifetime of the ESPT structure to be precisely determined but is nevertheless shorter than 100 ps with 0.8 eV of excess energy.

In order to shed light on the photofragmentation selectivity observed in the pump-probe signal, vertical excitation energies from the singlet and triplet ESPT structures of the conformer A of $TrpH^+$ to higher excited states are reported in Table 1 along with their oscillator strengths. Note that the results are similar for the conformer B. The small but yet constant signal at long delay reveals that a long-lived population can absorb the probe photon at 450 nm but not at 650 nm. Since the ESPT is the lowest singlet excited state, we have also calculated the triplet states of the ESPT form which might account for this long lifetime. The molecular orbitals are depicted in Figure S4. The ESPT form has an ππ* electronic configuration with the electronic density centered on the protonated indole ring. The third and fourth excited states correspond to $n\pi_{ind}$* states with different electronic configurations of the lone pair. For S_3, the excitation of the lone pair orbital of the NH_2 group towards the π* orbital of the indole ring has a vertical excitation energy of 1.69 eV, thus compatible with laser excitation at 650 nm. The S_4 state is characterized by the excitation of the lone pair orbital of the oxygen of the carboxylic acid group, with a vertical excitation energy of 2.72 eV (455 nm). The S_5 state is calculated at 3.14 eV (394 nm) and has a ππ* electronic configuration. These vertical excited state energies provide an upper limit for

Table 1. Electronic configuration, vertical excitation energies (eV) and oscillator strengths (*f*) of the excited states from the optimized ESPT singlet and triplet states ($^1\pi_1\pi^*$ and $^3\pi_1\pi^*$).

^{1}ESPT Elect. Conf.	Excitation energy [eV/nm]	*f*	^{3}ESPT Elect. Conf.	Excitation energy [eV/nm]	*f*
S_2 $^1\pi_2$ π*	1.08/1148	*0.007*	T_2 $^3\pi_2$ π*	1.06/1170	*0.008*
S_3 $^1n_{NH2}$ π*	1.69/738	*0.075*	T_3 $^3\pi_3$ π*	2.26/548	*0.034*
S_4 ^1n_O π*	2.72/455	*0.021*	T_4 $^3n_{NH2}$ π*	2.35/527	*0.049*
S_5 $^1\pi_3$ π*	3.14/394	*0.32*	T_5 ^3n_O π*	3.31/374	*0.016*

the adiabatic transition from the ESPT structure. The change in the fragmentation branching ratio as a function of the probe wavelength around 525 nm is tentatively explained by the different excited states reached by the probe photon from the ESPT form. It would imply that the $n_{NH2}\pi^*$ state is involved in the specific C_α-N bond cleavage (m/z 188) observed at 650 nm. For the opening of the C_α–C_β bond cleavage (m/z 130) at 525 nm, we cannot assert which of the $n_O\pi^*$ state or $\pi\pi^*$ state triggers such specific photofragment. In any case, a back proton transfer to the nitrogen that has kept a sp^3 hybridization prone to accept the proton occurs in the course of formation of the photofragments. However, the precise photo fragmentation processes in the excited state are out of the scope of the present study. Finally, the adiabatic excitation energy of the T_1 $^3\pi\pi^*$ state of the ESPT form is calculated at 2.90 eV, so 1.45 eV below the onset of the broad excitation band of $TrpH^+$. The first electronic transitions with significant oscillator strengths from the T_1 of the ESPT form are calculated at about 520–550 nm. This could explain why the long-lived excited state is not observed with the probe laser set at 650 nm.

Spectroscopy of $TrpH^+$–H_2O

UVPD Mass Spectrum and Spectroscopy

The UV photodissociation mass spectrum and excitation spectrum of $TrpH^+$–H_2O (m/z 223) are reported in Figure 2. When excited in the region of the band origin around 35 200 cm^{-1}, m/z 131 is the main fragmentation channel that is associated with the C_α–C_β bond cleavage and m/z 188 is a minor fragment that is formed after water evaporation and ammonia loss. A few hundred wavenumbers to the blue of the band origin, the fragmentation branching ratio drastically changes with the closure of the m/z 131 channel and the increase of signal at m/z 188. The UVPD spectrum of $TrpH^+$–H_2O monitored on the detection of these two fragments is reported in Figure 2b. As it can be readily seen, the vibronic pattern observed on these two fragments is completely different. Sharp and well-structured vibronic transitions are detected on the m/z 131 fragment with a band origin at 35 177 cm^{-1} (labeled A) that extends in a narrow spectral range up to 35 400 cm^{-1}. Conversely, a broad, unstructured band is observed on the m/z 188 fragment, which starts slightly to the red around 35 000 cm^{-1} (labeled B). This broad excitation spectrum was indeed observed by Mercier *et al.*[23] when monitoring the m/z 188 photofragment. Around 35 450 cm^{-1}, sharp vibronic transitions appears on the top of a weak intensity background signal. For instance, intense vibronic peaks are observed at 35 607 cm^{-1} (labeled C) and 35 917 cm^{-1} (labeled D), so 430 cm^{-1} and 740 cm^{-1} from the band origin. However, it cannot be concluded at this stage whether the broad absorption band is issued from homogeneous broadening or bad Franck-Condon factors. Double resonance IR-UV and pump-probe excited state dynamics are presented below to decode this unusual spectroscopic pattern.

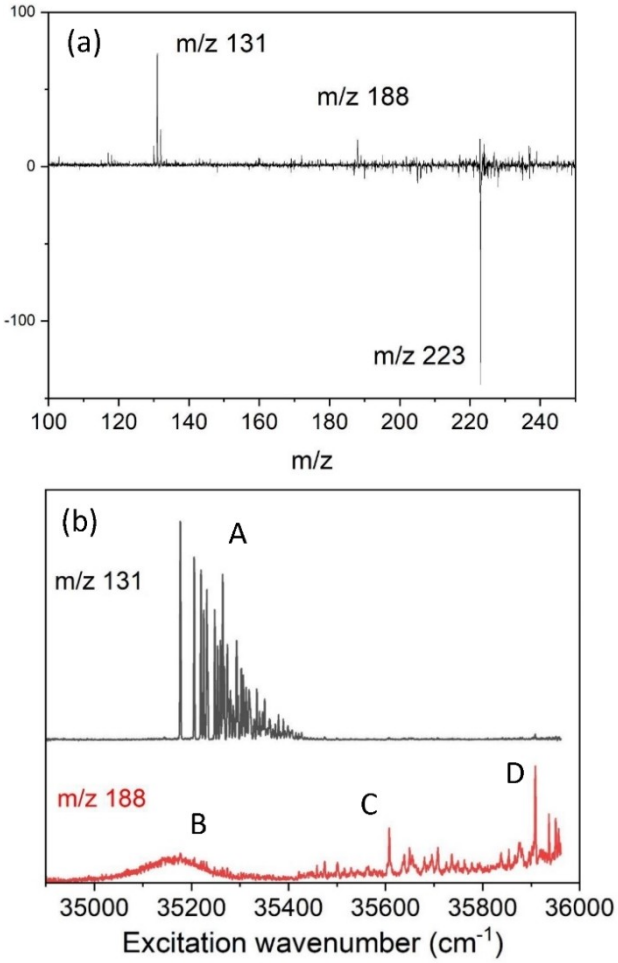

Figure 2. (a) Difference mass spectrum (laser on – laser off) at 35 177 cm^{-1} and (b) UVPD spectrum of $TrpH^+$–H_2O recorded on the photofragments m/z 131 and m/z 188.

IR-UV Hole Burning Spectra and Conformer Assignment

The totally different vibronic spectra recorded on the two main photofragments of $TrpH^+$–H_2O suggests that at least, two conformers with drastic different photophysical properties are populated after cryogenic cooling. IR-UV dip spectra are plotted in Figure 3 from 3000 to 3800 cm^{-1} with the UV set at 35177 cm^{-1} (conf A) detected on the depleted signal at m/z 131 and with the UV set at 35 160 cm^{-1}, i.e. within the broad absorption band (conf B), detected on the depleted signal at m/z 188.

The IR dip spectrum shown in Figure 3a is composed of 4 intense transitions at 3701 cm^{-1}, 3557 cm^{-1}, 3546 cm^{-1}, 3503 cm^{-1} plus a broader band centered at 3190 cm^{-1} with two shoulders on both sides. Interestingly, the IR dip spectra while probing the band C and D are exactly similar to the spectrum probing A (Figure S5) This means that these vibronic transitions belong to the same conformer, noted A. The IR-UV hole burning spectrum in which the UV is scanned while the IR wavelength is set at 3701 cm^{-1} is reported in Figure S6 along with the UV-UV hole burning spectrum in which the UV burn laser is set at the

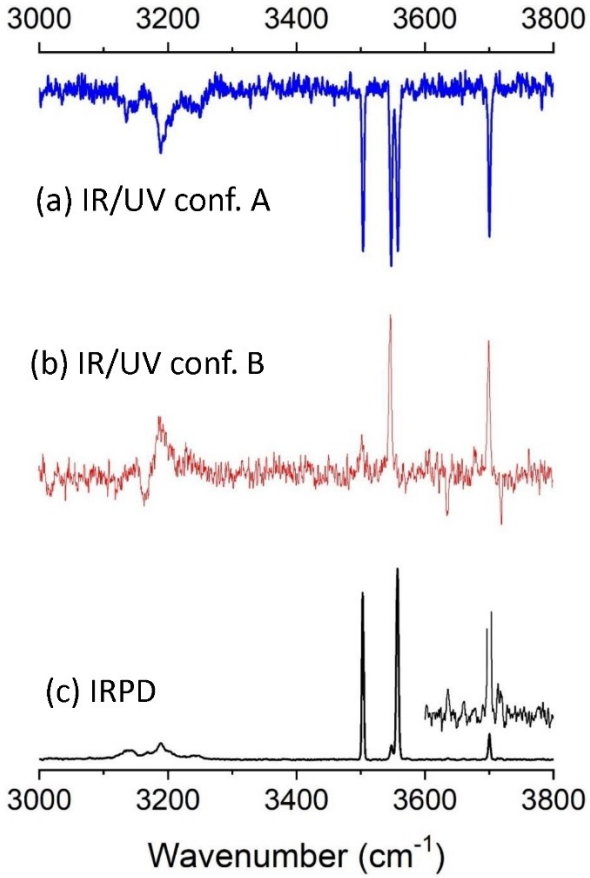

Figure 3. (a, b) IR-UV hole burning spectra of $TrpH^+$–H_2O probing the band A and band B of the UVPD spectrum, respectively. (c) IRPD spectrum. Insert is a zoom of the region around 3700 cm^{-1}.

band origin of conformer A. All the vibronic transitions observed in the UVPD spectrum while monitoring the m/z 131 fragmentation channel are depleted in both cases, which unambiguously proves that a single conformer contributes to the well-resolved vibronic spectrum associated with conformer A. Finally, the IR-UV spectrum of $TrpH^+$-D_2O (heavy water) reported in Figure SI7 misses the bands at 3546 cm^{-1} and 3701 cm^{-1} that are thus assigned to the symmetric and asymmetric H_2O stretches, respectively.

The IR-UV spectrum shown in Figure 3b is clearly different, with dips at 3719 cm^{-1}, 3636 cm^{-1} and 3160 cm^{-1} that are specific to another conformer, along with an increase of signal at 3701 cm^{-1}, 3546 cm^{-1}, 3503 cm^{-1} and 3190 cm^{-1}. It is noteworthy that IR frequencies at which the increase of the fragmentation signal at m/z 188 are observed exactly match the ones of the conformer A. Such positive signal in the IR-UV spectroscopy is most likely due to hot conformer A that produces a gain signal detected at m/z 188 as could be observed in IR-UV gain spectroscopy.[32]

Finally, the IRPD spectrum of $TrpH^+$–H_2O, monitored on the m/z 205 photofragment (H_2O evaporation), is reported in Figure 3c. This spectrum closely resembles the one reported by Spieler *et al.*[33] but at a slightly better resolution, so close lying frequency modes can now be distinguished. The IRPD spectrum comprises all the transitions observed in the two IR-UV dip spectra. It can thus be confidently concluded that only two conformers are populated in the cold ion trap. Although the band positions are the same in the IRPD and IR-UV dip spectra, their relative intensities are distinct. For instance, bands at 3701 cm^{-1} and 3546 cm^{-1} are barely seen in the IRPD spectrum while transitions at 3503 cm^{-1} and 3557 cm^{-1} are very intense. These latter are very close to the free indole NH and carboxylic OH stretches recorded for bare $TrpH^+$.[32] Such intensity alteration between IRPD and IR-UV hole burning spectra has already been observed and discussed.[34] This is related to the so-called IRPD transparency effect.[35] While hole burning spectroscopy depends linearly on the absorption of one IR photon to deplete the ground state population, IRPD requires multiphoton absorption within the laser pulse to reach a dissociation limit. Because dissociation limits are most of the time higher than transition states for isomerization, after the absorption of the first IR photon, the molecular system will first explore the potential energy surface to isomerize. Only modes that have a frequency independent of the conformation would be able to reabsorb a photon that will trigger photodissociation. For $TrpH^+$–H_2O, the indole NH stretch and the carboxylic OH stretch fulfill such condition.

In order to assign the structures of the $TrpH^+$–H_2O complex, conformational search has been performed from the two conformers A and B of $TrpH^+$ with one water. As expected, the lowest energy structures of the $TrpH^+$–H_2O complex comprise a direct interaction of the water around the ammonium within three types of arrangement, in between the indole ring, on the side or on the top of the ammonium. The structures along with the relative energy of each conformer are reported in Figure 4 and their predicted IR spectra are compared to the two experimental spectra in Figure 5. Regarding the energetics, the six conformers are predicted within less than 1 kcal/mol. Besides, the ordering between the different conformers differs from 0 K to ΔG_{180K} calculations. The free energy is calculated at 180 K which corresponds to the temperature of the clustering trap. If min4 and min6 lie systematically at higher energy, none of the 4 others could be discarded by this criterion.

The predicted IR spectra provide some clues to assign the structures. First, all conformers have predicted indole NH stretch and carboxylic OH stretch within 2–3 cm^{-1} from each other, at 3503 cm^{-1} and 3555 cm^{-1}, respectively. As these two groups are not involved in intermolecular H-bond with water, their respective frequencies are calculated very close to those of bare $TrpH^+$. This also further confirms the first assignment based on the IRPD spectrum. These two modes, which have their frequency independent of the conformation are the ones with the highest IRPD intensity. Second, in the 3550–3700 cm^{-1} spectral region, the two others observed transitions are thus assigned to the symmetric and asymmetric H_2O stretches, which are clearly distinct from conformers A and B. Min1, and to a less extent min4, the two conformers for which the water molecule is inserted in between the ammonium and the indole ring, provide the best match with the experimental spectrum of conformer A, in particular the close proximity of the H_2O

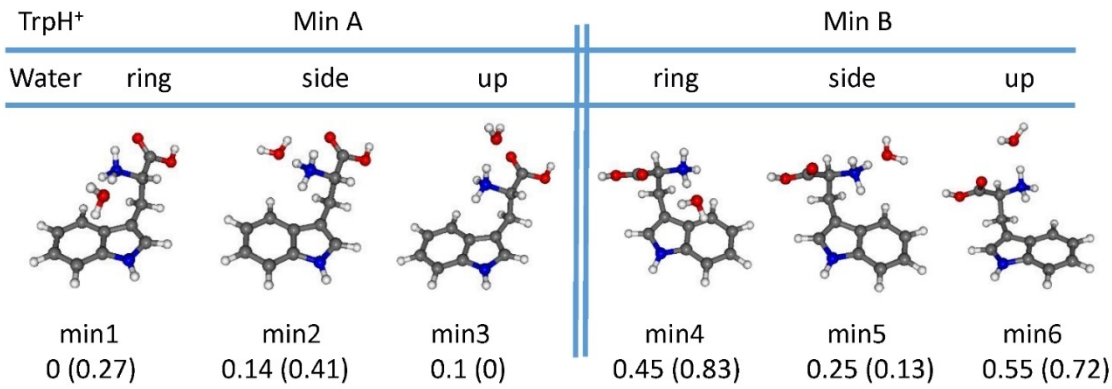

Figure 4. Lowest energy conformers of $TrpH^+$–H_2O. Relative energy E + ZPE and free energy (ΔG_{180K}) in kcal/mol.

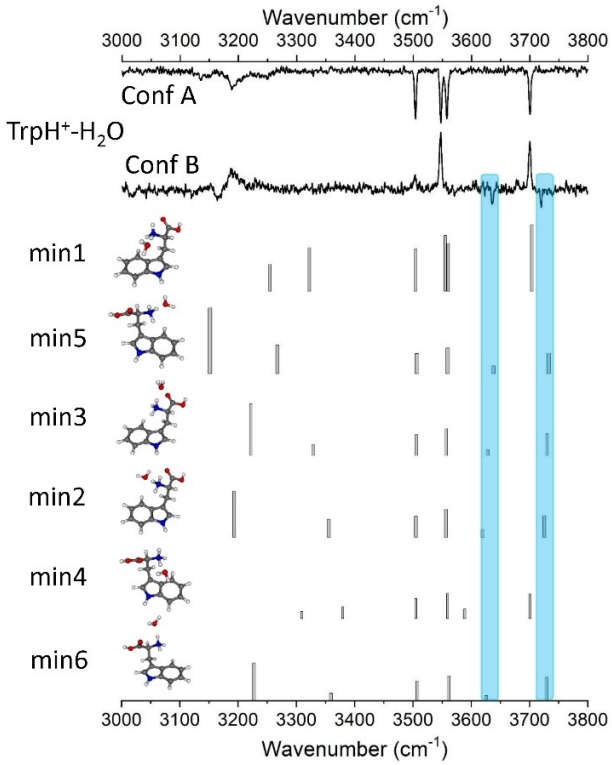

Figure 5. Comparison between calculated and experimental spectra of $TrpH^+$–H_2O. The blue shaded boxes highlight the symmetric and asymmetric H_2O stretches that discriminates conformer B from conformer A.

symmetric stretch with the carboxylic OH mode. Conversely, the 4 others conformations have blue-shifted H_2O symmetric and asymmetric stretches, in qualitative agreement with the IR spectrum of conformer B. However, as it can be checked in Figure 5, the spectral differences between these 4 conformers are too small to allow a firm assignment. Finally, the broad band around 3150–3250 cm^{-1} is assigned to the NH stretches of the NH_3^+ moiety, except the NH bond involved in H-bonding with the water that is predicted further to the red (not reported). The large red shift of the NH_3^+ modes makes the assignment based on harmonic calculations tendentious.[33]

Excited state dynamics of $TrpH^+$–H_2O

Picosecond pump-probe photodissociation dynamics

In order to record the excited state lifetime of the two conformers of $TrpH^+$–H_2O, ps pump-probe photodissociation spectroscopy was performed as for the bare molecule. The ps UV spectrum of $TrpH^+$–H_2O, monitoring the two fragmentation channels m/z 188 and m/z 131 is reported in Figure SI8. Although the vibronic pattern observed on the m/z 131 fragment cannot be resolved due to the larger bandwidth of the ps laser (10 cm^{-1}), the set of two bands assigned to conformers A and B can be separated. In Figure 6 are reported the transients recorded at two pump wavelengths exciting selectively conformers A and B (see Figure SI8). These two transients have been fitted with a single exponential decay function. For the conformer A, the probe wavelength is set at 650 nm, the transient is monitored on the depletion of the m/z 131 fragment. For the conformer B, the probe laser is set at 450 nm, and the transient is recorded on the 2-color fragment m/z 130, as done for $TrpH^+$. This set of two probe wavelengths provides the best 2-color signal to noise ratio for each conformer.

As expected from the well-resolved steady-state excitation spectrum recorded for conformer A, the excited state lifetime exhibits a time constant on the order of nanoseconds, highlighting a minimum in the Franck Condon region of the π-π* transition of conformer A. However, conformer B shares the

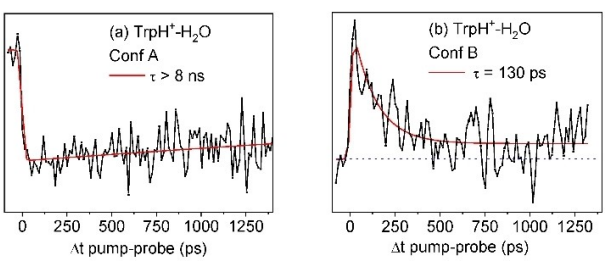

Figure 6. Pump-probe photodissociation transients recorded for the conformers A and B of $TrpH^+$–H_2O.

same broad absorption band and transient as bare $TrpH^+$. The unresolved vibronic spectrum is attributed to an ultrafast deactivation process of the ππ* state, probably leading to the ESPT structure with a lifetime of about 100 ps. For the conformer B, it is noteworthy that a constant signal is detected at long time delays as for $TrpH^+$ when the probe wavelength is set at 450 nm.

Excited-State Calculations

Excited state optimizations and frequency calculations at the SCS-CC2/aug-cc-pVDZ level were performed for the six lowest energy conformers of $TrpH^+$–H_2O. For all conformers, the first excited state S_1 corresponds to a π-π* transition. Unlike to the case of bare $TrpH^+$, S_1 geometry optimization leads to a minimum of the PES for all conformers except for min5 that displays a barrierless ESPT reaction. The adiabatic excitation energies, corrected by the difference of zero-point energy, are reported in Table 2. For min5, the ESPT reaction is exothermic with about the same energetics as for the bare $TrpH^+$, its adiabatic energy being calculated at 3.54 eV, so about 0.8 eV below the onset of the broad absorption band. Therefore, both the ground state vibrational spectrum and excited state property of min5 are consistent with the experimental findings recorded for conformer B that thus provides a firm assignment. The five others conformers have predicted adiabatic excitation energy at 4.3 ± 0.02 eV, very close to the experimental energy of 4.36 eV. Since min1 provides the best agreement with the ground state vibrational spectrum, we assign min1 to conformer A. Finally, min 3, which has the lowest Gibbs energy at 180 K, is not observed experimentally. Note that the energy difference between min1, min3 and min5 is less than 0.3 kcal/mol, thus within the uncertainty of the method. In addition, the entropic contribution of min3, which has a labile water molecule above $TrpH^+$, may be overestimated compared to min1, for which the water is constrained between the ammonium and indole groups.

Conformer-Specific Photofragmentation Channels

The last striking result is related to the specific photofragments detected for each conformer of Trp–H_2O when excited at their band origin. When probing the conformer B, the photofragmentation channel m/z 188 is issued from the H_2O evaporation and NH_3 loss. Compared to $TrpH^+$, the m/z 188 fragment is now stable within tens of ms, which is certainly due to the evaporating cooling of the water molecule which releases at least its binding energy calculated at 0.7 eV at the CC2 level.

Table 2. Adiabatic excitation energies (eV) corrected by the difference in zero-point energy (SCS-CC2/aug-cc-pVDZ) of the 6 lowest energy conformers of $TrpH^+$–H_2O.

	Min1	Min2	Min3	Min4	Min5	Min6
S_1	4.28	4.32	4.31	4.29	3.6 (ESPT)	4.31

This fragmentation channel strongly suggests that internal conversion to the ground state occurs as observed in the bare $TrpH^+$. In both cases, a barrierless ESPT is predicted leading to a stable minimum of the PES, with an energy gap with the ground state calculated around 1.5–2 eV. The exothermicity of the ESPT reaction is calculated at 0.60 eV, providing enough internal energy to eventually reach a point of the PES where the excited and ground state cross. The lifetime of the ESPT structure is within 100 ps. We cannot assert, however, whether or not the dynamics of water evaporation in the excited state contributes to this transient.

For the conformer A of $TrpH^+$–H_2O, the C_α–C_β bond break channel is observed only near the band origin. It is noteworthy that the ionic fragment at m/z 131 bears an extra hydrogen, revealing that a proton transfer has ultimately occurred. This specific fragmentation channel closes 300 cm^{-1} above the band origin, the vibronic spectroscopy of the ππ* state being still detected but through another fragmentation channel m/z 188. Such evolution of the fragmentation branching ratio between C_α–C_β bond break near the band origin and the opening of another fragmentation channel with the increase of excess energy in the excited state has already been observed in related systems, such as $TyrH^+$, $PheH^+$ and $AdeH^+$.[13,15] In these former cases, it was proposed that the C_α–C_β bond break was triggered by the ESPT reaction since the resulting photofragment bears an extra proton. Besides, in the course of the ESPT reaction, crossing with the ground state is predicted in these three species, at odds with the stable ESPT structure found for $TrpH^+$ for instance. When reaching the S_1/S_0 seam, competition between direct dissociation in the excited state leading to C_α–C_β bond cleavage or internal conversion to the ground state could explain the change in the fragmentation branching ratio with the excess energy imparted in the excited state. This subtle evolution of the fragmentation branching ratio within a small energy range deserves high-level excited state calculations that are beyond the scope of this study.[36]

Conclusion

By combining IR, UV cryogenic ion spectroscopy with time-resolved excited state dynamics, we have provided a comprehensive picture of the photoinduced dynamics of $TrpH^+$ and its mono hydrate, supported by quantum chemistry calculations. We have measured the transient spectroscopy associated with the ESPT reaction occurring in $TrpH^+$ excited at the band origin. The ESPT structure, reached with about 0.8 eV of excess energy, has a lifetime shorter than 100 ps. A small but yet constant signal in detected in the transient spectroscopy, which is assigned to the triplet state of the ESPT form. Interestingly, the fragmentation channel of $TrpH^+$ could be changed using different probe wavelengths, revealing the involvement of distinct excited states with different electronic configurations that trigger specific photofragmentation. In the mono hydrated species, two conformers have been assigned through comparison with ground state and excited state calculations. In one of them, a barrierless ESPT reaction occurs as in the bare $TrpH^+$,

leading to the same photofragment m/z 188. The striking result arises from the detection of a second conformer with well-resolved vibronic spectroscopy whose excited state lifetime is in the nanosecond range. Besides, this conformer has a specific UV photofragmentation channel at m/z 131, issued from the C_α–C_β bond cleavage. This fragmentation channel closes 300 cm^{-1} above the band origin where the CID-like fragment at m/z 188 (H_2O and NH_3 loss) is then observed.

This spectroscopic study points out the subtle photodynamics occurring already in the mono hydrated $TrpH^+$. A single water molecule interacting at a specific site in between the ammonium and the indole ring can efficiently block the barrierless ESPT reaction. This local, yet drastic environment effect clearly validates the use of cryogenic ion spectroscopy on mass and conformer-selected species to decipher the complex photophysics of UV chromophores that are widely used to study larger peptides and proteins in solution. These benchmarks experimental results should foster computational studies focusing on exited state PES and non-radiative deactivation processes including internal conversion, intersystem crossing and photochemistry in the vicinity of conical intersection.

Experimental and Computational Section

The experimental setup in Orsay[17] has been upgraded with the addition of a temperature-controlled clustering trap to produce hydrated species, as already done in Tokyo.[37,38] It now comprises on an electrospray ion source, a liquid-nitrogen cooled octopole (clustering trap), a quadrupole mass filter (from ThermoFisher company with specially designed electronics from JanasCard, Czech Republic), a cryogenic cooled 3D quadrupole ion trap (QIT, Jordan TOF Inc) and a home-made linear time-of-flight mass spectrometer. A water/methanol solution (1:1) of Trp (100 μM) is electrosprayed in front of a heated capillary, the produced ions are then transferred into an octopole through a skimmer and stored for 100 ms. A bunch of ions is extracted from the octopole by a pulsed electrode and accelerated at 200 V and transferred into the clustering trap biased at 200 V and housed in a copper box which is mounted on a cold head of a liquid nitrogen cryostat (Janus). Water vapor is introduced by a pulsed valve (Parker Hannifin, General Valve Series 9) triggered a few ms before the entering of the ions and the temperature of the octopole is maintained at about 180 K, which provides the best compromise for the production of the singly hydrated $TrpH^+$ while avoiding the formation of larger cluster sizes. The hydrated species are extracted from the octopole after a few ms, mass-selected by a quadrupole mass filter that transfers the ions directly into the Paul Trap. The QIT is biased at 200 V to avoid dissociations of the incoming species through collisions with the buffer gas and mounted on a cold head of a compressed helium cryostat (CH-204S, Sumitomo) that maintains the temperature around 15 K. The mass-selected complexes are stored and thermalized through collisions with helium buffer gas injected by a pulsed valve (Parker, general valve) a few ms before the entering of the ions. Parent ions and photofragments, produced as described below, are mass-analyzed in a linear TOF-MS and detected by microchannel plates (Z-Gap, Jordan TOF Inc).

The ps pump-probe photodissociation experiments were conducted in Orsay, using the outputs of two OPA (EKSPLA-PG411) pumped by a mode-locked picosecond Nd:YAG laser (EKSPLA-SL300). The cross-correlation of the pump and probe pulses is 16 ps and the two lasers pulses are delayed by a motorized optically delay line scanned in 6.6 ps step up to 1400 ps. The steady-state UV and IR spectroscopies were performed in Tokyo with a tunable dye UV laser (Lumonics) and a OPO/OPA IR laser (LaserVision). UV/IR photodissociation (UVPD/IRPD) spectra were measured by scanning the yield of the photofragment ions as a function of laser wavenumber. For the hydrates, the moderate binding energies of the water molecule with $TrpH^+$ allow recording IRPD spectroscopy by monitoring the water evaporation channel as a function of the IR wavelength. To measure an IR-UV dip spectrum, the tunable IR laser illuminated the hydrated ions before UV irradiation whose wavenumber was fixed at the band origin of the UVPD spectrum of a given conformer. If the ions are vibrationally excited by the IR laser, the photofragment yield is reduced due to the depopulation of the ground vibrational state. IR-UV dip spectra were thus obtained by monitoring the depletion of the UV photofragment signal and gives conformer-selective IR spectra.

Conformational search of $TrpH^+$–H_2O was performed with the xtb program by semi empirical tight-binding methods using the conformer rotamer ensemble sampling tool (crest) module.[39] The ground-state vibrational spectra of $TrpH^+$–H_2O have been simulated at the DFT/B3LYP-D3BJ/cc-pVTZ level using Gaussian 16.[40] The harmonic frequencies are corrected with a global scaling factor of 0.961 for all modes. For the excited states, coupled-cluster calculations have been performed with the TURBOMOLE program package (v7.1)[41] making use of the resolution-of-the-identity (RI) approximation for the evaluation of the electron-repulsion integrals.[42,43] The equilibrium geometries of protonated tryptophan and its water cluster in the electronic ground (S_0) and first excited (S_1 and T_1) states have been determined at the spin-component scaled SCS-CC2 level[44–46] with correlation-consistent polarized valence double-ζ aug-cc-pVDZ basis set augmented with diffuse functions.[47] For the SCS-CC2 calculations, we used the standard scaling factors as implemented in Turbomole (css = 1/3, cos = 6/5). The vibrational modes of the ground and the first excited states have been calculated at the same level in order to obtain the adiabatic excitation energy corrected for the difference of zero-point energy between the two states.

Acknowledgements

This work was supported in part by the "ADI 2019" project funded by the IDEX Paris-Saclay, ANR-11-IDEX-0003-02, KAKENHI (JP19K23624, JP20K20446, JP20H00372, JP21H04674, and JP21K14585), the Core-to-Core program (JPJSCCA20210004) from the Japan Society for the Promotion of Science of JSPS, the World Research Hub Initiatives in Tokyo Institute of Technology, the Cooperative Research Program of the "Network Joint Research Center for Materials and Devices" from the Ministry of Education, Culture, Sports, Science and Technology (MEXT), Japan. The computations were performed at the HPC resources from the "Mésocentre" computing center of CentraleSupelec and Ecole Normale Supérieure Paris-Saclay supported by CNRS and Région Ile-de-France (https://mesocentre.centralesupelec.fr/) and the HPC resources MAGI from University Paris 13.

Conflict of Interest

The authors declare no conflict of interest.

Data Availability Statement

The data that support the findings of this study are available from the corresponding author upon reasonable request.

Keywords: cryogenic ion spectroscopy · IR and UV photodissociation · biomolecules · hydration · photophysics

[1] J. R. Lakowicz, Ed., *Principles of Fluorescence Spectroscopy*, Springer US, Boston, MA, **2006**.
[2] C. A. Royer, *Chem. Rev.* **2006**, *106*, 1769–1784.
[3] Y. Chen, M. D. Barkley, *Biochemistry* **1998**, *37*, 9976–9982.
[4] J. T. Vivian, P. R. Callis, *Biophys. J.* **2001**, *80*, 2093–109.
[5] L. Blancafort, D. González, M. Olivucci, M. A. Robb, *J. Am. Chem. Soc.* **2002**, *124*, 6398–6406.
[6] C.-P. Pan, P. L. Muiño, M. D. Barkley, P. R. Callis, *J. Phys. Chem. B* **2011**, *115*, 3245–3253.
[7] O. V. Boyarkin, *Int. Rev. Phys. Chem.* **2018**, *37*, 559–606.
[8] S. Soorkia, C. Jouvet, G. Grégoire, *Chem. Rev.* **2020**, *120*, 3296–3327.
[9] H. Kang, C. Jouvet, C. Dedonder-Lardeux, S. Martrenchard, G. Grégoire, C. Desfrançois, J.-P. Schermann, M. Barat, J. A. Fayeton, *Phys. Chem. Chem. Phys.* **2005**, *7*, 394.
[10] V. Lepère, B. Lucas, M. Barat, J. A. Fayeton, V. J. Picard, C. Jouvet, P. Çarçabal, I. Nielsen, C. Dedonder-Lardeux, G. Grégoire, A. Fujii, *J. Chem. Phys.* **2007**, *127*, 134313.
[11] O. V. Boyarkin, S. R. Mercier, A. Kamariotis, T. R. Rizzo, *J. Am. Chem. Soc.* **2006**, *128*, 2816–7.
[12] G. Grégoire, C. Jouvet, C. Dedonder, A. L. Sobolewski, *J. Am. Chem. Soc.* **2007**, *129*, 6223–6231.
[13] G. Féraud, M. Broquier, C. Dedonder, C. Jouvet, G. Grégoire, S. Soorkia, *J. Phys. Chem. A* **2015**, *119*, 5914–5924.
[14] H. Wako, S. Ishiuchi, D. Kato, G. Féraud, C. Dedonder-Lardeux, C. Jouvet, M. Fujii, *Phys. Chem. Chem. Phys.* **2017**, *19*, 10777–10785.
[15] J. Dezalay, M. Broquier, S. Soorkia, K. Hirata, S. Ishiuchi, M. Fujii, G. Grégoire, *Phys. Chem. Chem. Phys.* **2020**, *22*, 11498–11507.
[16] R. Antoine, M. Broyer, C. Dedonder, C. Desfrancois, C. Jouvet, D. Onidas, P. Poulain, T. Tabarin, P. Dugourd, G. Gregoire, G. Van Der Rest, *Rapid Commun. Mass Spectrom.* **2006**, *20*, 1648–1652.
[17] M. Broquier, S. Soorkia, G. Grégoire, *Phys. Chem. Chem. Phys.* **2015**, *17*, 25854–25862.
[18] K. Hirata, K. Kasai, G. Grégoire, S. Ishiuchi, M. Fujii, *J. Chem. Phys.* **2021**, *155*, 151101.
[19] H. Kang, C. Dedonder-Lardeux, C. Jouvet, G. Grégoire, C. Desfrançois, J.-P. Schermann, M. Barat, A. Fayeton, *J. Phys. Chem. A* **2005**, *109*, 2417–2420.
[20] F. O. Talbot, T. Tabarin, R. Antoine, M. Broyer, P. Dugourd, *J. Chem. Phys.* **2005**, *122*, 074310.
[21] H. Kang, C. Dedonder-Lardeux, C. Jouvet, S. Martrenchard, G. Grégoire, C. Desfrançois, J.-P. Schermann, M. Barat, J. A. Fayeton, *Phys. Chem. Chem. Phys.* **2004**, *6*, 2628–2632.
[22] S. Soorkia, M. Broquier, G. Grégoire, *J. Phys. Chem. Lett.* **2014**, *5*, 4349–4355.
[23] S. R. Mercier, O. V. Boyarkin, A. Kamariotis, M. Guglielmi, I. Tavernelli, M. Cascella, U. Rothlisberger, T. R. Rizzo, *J. Am. Chem. Soc.* **2006**, *128*, 16938–16943.
[24] K. Hirata, K.-I. Kasai, K. Yoshizawa, G. Grégoire, S.-I. Ishiuchi, M. Fujii, *Phys. Chem. Chem. Phys.* **2022**, *24*, 10737.
[25] H. El Aribi, G. Orlova, A. C. Hopkinson, K. W. M. Siu, *J. Phys. Chem. A* **2004**, *108*, 3844–3853.
[26] H. Lioe, R. A. J. O'Hair, G. E. Reid, *J. Am. Soc. Mass Spectrom.* **2004**, *15*, 65–76.
[27] W. K. Mino, K. Gulyuz, D. Wang, C. N. Stedwell, N. C. Polfer, *J. Phys. Chem. Lett.* **2011**, *2*, 299–304.
[28] G. Grégoire, B. Lucas, M. Barat, J. A. Fayeton, C. Dedonder-Lardeux, C. Jouvet, *Eur. Phys. J. D* **2009**, *51*, 109–116.
[29] V. Ovejas, M. Fernández-Fernández, R. Montero, A. Longarte, *Chem. Phys. Lett.* **2016**, *661*, 206–209.
[30] G. Grégoire, M. Mons, I. Dimicoli, F. Piuzzi, E. Charron, C. Dedonder-Lardeux, C. Jouvet, S. Martrenchard, D. Solgadi, A. Suzor-Weiner, *Eur. Phys. J. D* **1998**, *1*, 187–192.
[31] D. J. Hadden, C. A. Williams, G. M. Roberts, V. G. Stavros, *Phys. Chem. Chem. Phys.* **2011**, *13*, 4494–4499.
[32] A. Y. Pereverzev, X. Cheng, N. S. Nagornova, D. L. Reese, R. P. Steele, O. V. Boyarkin, *J. Phys. Chem. A* **2016**, *120*, 5598–5608.
[33] S. Spieler, C. H. Duong, A. Kaiser, F. Duensing, K. Geistlinger, M. Fischer, N. Yang, S. S. Kumar, M. A. Johnson, R. Wester, *J. Phys. Chem. A* **2018**, *122*, 8037–8046.
[34] N. Nieuwjaer, C. Desfrançois, F. Lecomte, B. Manil, S. Soorkia, M. Broquier, G. Grégoire, *J. Phys. Chem. A* **2018**, *122*, 3798–3804.
[35] T. I. Yacovitch, N. Heine, C. Brieger, T. Wende, C. Hock, D. M. Neumark, K. R. Asmis, *J. Phys. Chem. A* **2013**, *117*, 7081–7090.
[36] L. Blancafort, *ChemPhysChem* **2014**, *15*, 3166–3181.
[37] S. I. Ishiuchi, H. Wako, D. Kato, M. Fujii, *J. Mol. Spectrosc.* **2017**, *332*, 45–51.
[38] E. Sato, K. Hirata, J. M. Lisy, S. I. Ishiuchi, M. Fujii, *J. Phys. Chem. Lett.* **2021**, *12*, 1754–1758.
[39] P. Pracht, F. Bohle, S. Grimme, *Phys. Chem. Chem. Phys.* **2020**, *22*, 7169–7192.
[40] Gaussian 16 (Revision A.03), M. J. Frisch, G. W. Trucks, H. B. Schlegel, G. E. Scuseria, M. A. Robb, J. R. Cheeseman, G. Scalmani, V. Barone, G. A. Petersson, H. Nakatsuji, X. Li, M. Caricato, A. V. Marenich, J. Bloino, B. G. Janesko, R. Gomperts, B. Mennucci, H. P. Hratchian, J. V. Ortiz, A. F. Izmaylov, J. L. Sonnenberg, D. Williams-Young, F. Ding, F. Lipparini, F. Egidi, J. Goings, B. Peng, A. Petrone, T. Henderson, D. Ranasinghe, V. G. Zakrzewski, J. Gao, N. Rega, G. Zheng, W. Liang, M. Hada, M. Ehara, K. Toyota, R. Fukuda, J. Hasegawa, M. Ishida, T. Nakajima, Y. Honda, O. Kitao, H. Nakai, T. Vreven, K. Throssell, J. A. Montgomery, Jr., J. E. Peralta, F. Ogliaro, M. J. Bearpark, J. J. Heyd, E. N. Brothers, K. N. Kudin, V. N. Staroverov, T. A. Keith, R. Kobayashi, J. Normand, K. Raghavachari, A. P. Rendell, J. C. Burant, S. S. Iyengar, J. Tomasi, M. Cossi, J. M. Millam, M. Klene, C. Adamo, R. Cammi, J. W. Ochterski, R. L. Martin, K. Morokuma, O. Farkas, J. B. Foresman, D. J. Fox, Gaussian, Inc., Wallingford CT, **2016**.
[41] *TURBOMOLE V7.1, Dev. Univ. Karlsruhe Forschungszentrum Karlsruhe GmbH, 1989–2007, TURBOMOLE GmbH, since 2007; available from http//www.turbomole.com*.
[42] O. Christiansen, H. Koch, P. Jørgensen, *Chem. Phys. Lett.* **1995**, *243*, 409–418.
[43] R. Ahlrichs, *Phys. Chem. Chem. Phys.* **2004**, *6*, 5119.
[44] C. Hättig, *J. Chem. Phys.* **2003**, *118*, 7751–7761.
[45] A. Köhn, C. Hättig, *J. Chem. Phys.* **2003**, *119*, 5021–5036.
[46] A. Hellweg, S. A. Grün, C. Hättig, *Phys. Chem. Chem. Phys.* **2008**, *10*, 4119.
[47] R. A. Kendall, T. H. Dunning, R. J. Harrison, *J. Chem. Phys.* **1992**, *96*, 6796–6806.

Manuscript received: July 29, 2022
Revised manuscript received: September 6, 2022
Accepted manuscript online: September 30, 2022
Version of record online: October 25, 2022